Available online at www.sciencedirect.com
SCIENCE DIRECT®
Journal of Colloid and Interface Science 286 (2005) 487–495
JOURNAL OF Colloid and Interface Science
www.elsevier.com/locate/jcis

Cell surface groups of two picocyanobacteria strains studied by zeta potential investigations, potentiometric titration, and infrared spectroscopy

Maria Dittrich *, Sabine Sibler

Swiss Federal Institute for Environmental Science and Technology, EAWAG, and Swiss Federal Institute of Technology, ETH, Limnological Research Center, 6047 Kastanienbaum, Switzerland

Received 18 October 2004; accepted 20 January 2005

Available online 10 March 2005

Abstract

In order to clarify the role of picocyanobacteria in aquatic biogeochemical processes (e.g., calcite precipitation), cell surface properties need to be investigated. An experimental study of the cell surface characteristics of two *Synechococcus*-type unicellular autotrophic picocyanobacterial strains was carried out. One strain was isolated from Lake Plön and contained phycocyanin, the other strain came from Lago Maggiore and was rich in phycoerythrin. Potentiometric titrations were conducted to determine the different types of sites present on the bacteria cell walls. Infrared spectroscopy allowed characterization of the various functional groups ($R–NH_2$, R–COOH, R–OH, $R–PO_2$) and investigations of zeta potential provided insight into the isoelectrical points of the strains. Titrations reveal three distinct sites on the bacterial surfaces of phycocyanin- and phycoerythrin-rich strains with pK values of $4.8 \pm 0.3/5.0 \pm 0.2$, $6.6 \pm 0.2/6.7 \pm 0.4$, and $8.8 \pm 0.1/8.7 \pm 0.2$, corresponding to carboxyl, phosphate, and amine groups with surface densities of $2.6 \pm 0.4/7.4 \pm 1.6 \times 10^{-4}$, $1.9 \pm 0.5/4.4 \pm 0.8 \times 10^{-4}$, and $2.5 \pm 0.4/4.8 \pm 0.7 \times 10^{-4}$ mol/g of dry bacteria. The deprotonation constants are similar to those of bacterial strains and site densities are also within an order of magnitude of other strains. The phycoerythrin-rich strain had a higher number of binding sites than the phycocyanin-rich strain. The results showed that picocyanobacteria may adsorb either calcium cations or carbonate anions and therefore strongly influence the biogeochemical cycling of calcite in pelagic systems.

Keywords: Cyanobacteria; Cell surface; *Synechococcus*

1. Introduction

Cyanobacteria are photosynthetic prokaryotes commonly found in soils and freshwater. They are an important component of marine phytoplankton and contribute significantly to the overall primary production in ecosystems of all climatic zones [1,2]. Cyanobacteria often dominate the picoplankton community in oligotrophic systems [3–6].

Picocyanobacteria are increasingly investigated due to their ecological significance [7]. Recent studies indicate that picoplankton plays an important role in calcite precipitation in oligotrophic lakes [8]. One possible mechanism is a two-step process, during which calcium cations first bind to the cell surface, followed by the diffusion of hydroxyl ions through the cell membrane as a result of an uptake of HCO_3^- by photosynthesis [9]. Although the observation of fast and reversible Ca adsorption on picocyanobacteria cells in in situ microscopic study [10] supports this mechanism, the detailed steps of the precipitation of minerals and cells remain unclear.

Knowledge of cell surface properties is crucial to understand the calcite precipitation. The concentrations and characteristics of proton-active carboxylic, phosphoric, phosphodiester, hydroxyl, and amine functional groups on cell sur-

* Corresponding author. Fax: +41-41-349-21-68.
E-mail address: dittrich@eawag.ch (M. Dittrich).

0021-9797/$ – see front matter
doi:10.1016/j.jcis.2005.01.029

faces play an extremely important role in this respect, as they are responsible for the surface binding capacity.

Despite numerous investigations carried out on cell surfaces during the last decade, a general model of cell surface characteristics does not exist. Most bacteria in marine and freshwater settings are Gram-negative [11]. Nevertheless, until the late 1990s investigations of solute adsorption onto microbial surfaces focused on Gram-positive aerobic bacteria such as *Bacillus* sp., e.g., [12–14]. These studies showed that metal–bacteria complexes had high thermodynamic stabilities, which are comparable to those of common organic ligands [15,16]. The free surface energy calculated from contact angle measurements on dry microbial lawns could not be related to the Gram-character of some bacterial strains [17]. Yee and Fein [18] proposed that all bacterial species might be represented by a simple generic thermodynamic model for purposes of modeling metal transport in natural environments.

However, Gram-positive and Gram-negative bacteria differ significantly in their cell membrane structure and composition. The cell walls of Gram-positive bacteria are relatively simple and consist predominantly of a rigid peptidoglycan framework. In contrast, the cell walls of Gram-negative bacteria are complex and have an outer membrane covering a thin layer of peptidoglycan [19]. Therefore studies focusing on Gram-positive species can only provide limited information regarding the properties of Gram-negative strains.

The number of studies examining the surface chemistry of Gram-negative bacteria has recently increased quite significantly [20–22]. It has been suggested that Gram-negative bacteria should have less reactive sites than Gram-positive cells [23]. However, Sokolov et al. [24] found that the site densities of Gram-negative *Shewanella putrefaciens* were higher than those of Gram-positive *Bacillus subtilis* [14]. On the other hand, Haas et al. [25] reported a stability constant of the uranyl ion on carboxyl sites that is almost three orders of magnitude lower than that for *Bacillus* cells [14]. The X-ray photoelectron spectroscopy (XPS) studies on dehydrated freeze-dried cells of 210 strains, showed that the Gram character of bacterial strains was not reflected in the group distribution of the elemental surface concentration ratios (N/C, O/C, and P/C) [26]. No convincing relationships have been found however for Gram-negative bacteria between XPS data and other physicochemical cell surface properties [27]. Therefore it is still unclear to what extent generalizations can be made about the cell surface properties of Gram-negative and -positive bacteria.

The objectives of the present study were to clarify this discrepancy by characterizing the surface of Gram-negative picocyanobacteria. The characterization of picocyanobacteria surface properties is necessary to reveal their role in the biogeochemistry of aquatic systems, particularly for mineral precipitation. Until now, the cell surface of small coccoid phototrophic picocyanobacteria has not been investigated in that respect. The aims of this study were to determine the identity, abundance, and acid-base properties of binding sites on the surfaces of two different picocyanobacteria strains.

A combination of in situ infrared spectroscopy, potentiometric titration, and zeta-potential measurements was carried out on intact cells of *Synechoccocus*-type blue-green phycocyanin (PC)-rich and red-pigmented phycoerythrin (PE)-rich strains. The experimental data were used to identify the dominant functional groups and to determine the concentration and acidity of the cell surface sites.

2. Methods

2.1. Picocyanobacteria growth

Green (rich in phycocyanin) and Red picocyanobacteria (rich in phycoerythrin) *Synechococcus*-type strains were used in all experiments presented here. The samples were isolated from the water column of two stratified lakes: the Plöner See and Lago Maggiore (courtesy of C. Callieri). Cells were grown as batch cultures using modified Z/10 medium (5.9 mg/l $Ca(NO_3)_2 \cdot 4H_2O$, 46.7 mg/l $NaNO_3$, 4.1 mg/l $K_2HPO_4 \cdot 3H_2O$, 2.5 mg/l $MgSO_4 \cdot 7H_2O$, 168 mg/l $NaHCO_3$, 11.45 mg/l Na-EDTA, 3 mg/l $FeSO_4 \cdot 7H_2O$, 248 µg/l H_3BO_3, 135 µg/l $MnSO_4 \cdot H_2O$, 7.2 µg/l $(NH_4)_6 \cdot Mo_7O_{24} \cdot 4H_2O$, 23.2 µg/l $ZnSO_4 \cdot 7H_2O$, 12 µg/l $Co(NO_3)_2 \cdot 6H_2O$, 10.4 µg/l $CuSO_4 \cdot 5H_2O$) under a 14 h/10 h light/dark condition, with a light intensity of approximately 10 µE/(m^2 s). Cells in the stationary growth phase were used for the titration experiments. Cell viability was verified using epifluorescence microscopy.

2.2. Preparation of cells

The cultures were harvested by centrifugation at 7000*g* for 10 min at 20 °C. The medium was decanted and the cells were resuspended in 0.001 M EDTA. After further centrifugation at 7000*g* for 10 min, the EDTA solution was decanted; the cells were resuspended in 0.1 M $NaNO_3$ and centrifuged under the same conditions listed above. The washing procedure in $NaNO_3$ was repeated four times and the cells were finally batched and resuspended in 50 or 10 ml of the 0.1 M $NaNO_3$.

2.3. Electrophoretic mobility investigations

The electrophoretic mobility of the suspensions was measured using a Zetasizer 3000, Malvern Instruments. The zeta potential was calculated from the measured mobility according to the Smoluchowski equation. Ready-to-use syringes with a zeta transfer potential standard (silica colloids) of -50 ± 5 mV from Malvern Instruments were used for calibration. Approximately 10 ml of washed bacterial suspension (0.5 g/l) was added to 0.1 M $NaNO_3$. The pH was adjusted to the required value using dilute HNO_3 or NaOH. The suspensions were stirred and conditioned until the pH

stabilized. The suspensions were then transferred to the electrophoresis cell for measurements. Approximately 10 readings were taken. The average values are reported here.

2.4. Potentiometric titration

2.4.1. Solutions

All solutions were prepared through analytical measurements to determine molar concentrations. The solutions were subsequently degassed with N_2 for 20 min to dissipate O_2 and CO_2. The $NaNO_3$ solutions were prepared by weighing a known amount of $NaNO_3$. The concentration of $NaNO_3$ used in this experiment was 0.1 M.

The NaOH solution was prepared according to the following method: approximately 0.1 M solution was prepared from NaOH using degassed 18 MΩ water. The exact NaOH concentration was determined prior to the titration experiment through the titration of three 5- or 10-ml aliquots with standard 0.1 M HCl. The three runs had a relative standard deviation of 1%.

2.4.2. Titrator setting

Deprotonation constants and surface site concentrations were determined from acid–base titrations of bacterial suspensions in a background electrolyte of 0.01 M $NaNO_3$. All titrations were performed in a glass vessel with a lid as part of a Metrohm GP 736 Titrino unit interfaced by Titrino software TITRINET to a personal computer. Two separate buret exchange units with 20 and 10 ml were used, one for the acid and one for the base. We also used a Metrohm titrator vessel lid. The temperature was recorded with a temperature sensor; the error of the temperature probe was 0.1 °C. The pH electrode was three-point calibrated with buffers (pH 4, 7, and 10) before each experiment, and the slope was consistently 99% of the Nernst value.

The Titrino unit was programmed with a dynamic mode (DYN) for the titration, which added the variable amount of titrant according to the pH changes: the smaller volume of titrant was added at the slope of the pH curve. The successive titrant additions were made only when the signal drift reached 10 mV/min.

2.4.3. Bacterial titration

The titrator electrode was first calibrated as mentioned above. The optical density (OD 630 nm) of the bacterial suspension in the $NaNO_3$ electrolyte solution was measured prior to each titration run. The measured absorbance was compared to a prepared calibration curve to determine the concentration of bacteria (in mg/l) and the bacterial cell numbers (cells/L). The dry weight of bacteria was defined by drying at 65 °C until a constant weight was attained. The absorbance used was in the range of 0.41–0.81, which corresponds to 0.063–0.122 g of bacteria/L. A known amount of bacterial suspension, approximately 50 ml, was then transferred to the titration vessel, which was immediately attached to the lid setup connected with the N_2 gas line. A magnetic stir bar was also added to the vessel. The whole system was then degassed for 30–40 min to exclude atmospheric CO_2. Following the degassing procedure a positive pressure of N_2 was maintained by allowing a gentle flow of N_2 into the headspace during the titration.

The bacterial aliquot was then titrated quickly to pH 2.9 with 0.1 M HCl. The buret exchange unit was subsequently changed and the titration of the aliquot with NaOH up to pH 10 began. The total time for each titration was approximately 40 min.

Some titrations were reversed by conducting an acid titration, which immediately followed the base titration. The results of reversed titrations were not significantly different from the forward titrations suggesting reversibility of the proton adsorption–desorption reactions.

2.5. Data analysis

The titration data are expressed in the form of charge excess versus $-\log[H^+]$, where the charge excess is calculated by the equation

$$[H^+]_{ex} = C_A - C_B - [H^+] + K_w/[H^+],$$

where C_A and C_B are concentrations of acid and base added, $[H^+]$ is obtained from the measured proton concentration, and K_w is the stability constant for the dissociation of water. It is necessary to model the H^+ exchanged due to deprotonation of sorption sites in order to determine pK_a values and site densities for binding sites on the bacteria surface. The acid–base titration experiments were modeled after the FITEQL 4 optimization routine [28] using the constant capacity model to determine the intrinsic deprotonation constants and surface site densities.

The specific surface area of *Synechococcus* was estimated using a geometric approach and measurements of external dimensions of viable bacteria by atomic force microscopy. The average long and short axes of *Synechococcus* PCC 7942 were measured at 2.3 and 0.5 µm, respectively. These particular size parameters of cells were used for all strains. Based on the estimation of the cell number from the optical density measurement and the known dry weight of the suspension from the relationship between weight and cell number, we obtained specific surface areas of 76 and 88 m^2/g for wet *Syn*. Green and *Syn*. Red strains, respectively.

The FITEQL 4 fits data to a specific function of variance $V(Y)$ between experimental data and the model

$$V(Y) = \frac{\sum\left(\frac{Y_{calc}-Y_{obs}}{S_{obs}}\right)^2}{n_p n_{II} - n_a}, \quad (1)$$

where Y_{calc} is the calculated value, Y_{obs} is the experimental value, S_{obs} is the error associated with the experimental data, n_p is the number of data points, n_a is the number of adjustable parameters in the model, and n_{II} is the number of components for which both the total and free (dissolved) concentrations are known.

The variance is thus a quantitative estimate of success in describing the data with a specified model. A value range of $0.1 < V(Y) < 20$ represents a good fit. Implicit in this modeling approach is the assumption that surface charge is homogeneously distributed over the bacterial surface, giving rise to a relatively simple behavior of the electric field. In this study, we neglect the effect of heterogeneities in the bacterial surface electric field, although previous studies on *Bacillus subtilis* revealed a higher concentration of surface sites on the bacteria tips [29].

2.6. Attenuated total reflectance infrared (ATR-IR) spectroscopy

ATR-IR measurements were performed on a Bio-Rad FTS 45 Fourier transformation infrared (FTIR) spectrophotometer with a 32000 data station. Scans ($n = 256$) with resolution 1 cm^{-1} were collected for each suspension spectrum of washed bacteria in 0.1 M $NaNO_3$. The suspension (appr. 0.5 g/l) was left to settle for 1–2 h; the spectra were then measured. The spectrum of 0.1 M $NaNO_3$ was used as a background. The base-line shift of the spectra was corrected using the MATLAB application (The Math Works, Inc., Natrick, MA, USA).

3. Results and discussion

3.1. Zeta potential of bacteria

The zeta potential measurements reveal that picocyanobacteria exhibit a net positive charge of the surface below a pH value of approximately 5 (Fig. 1). Unlike picocyanobacteria, the surfaces of investigated *Bacillus* sp. are negatively charged under broader pH conditions (2–8 [30]; 2.4–10 [31]). An isoelectric point of picocyanobacteria is approximately at pH 5. At this pH the concentration of negatively charged surface sites is equal to positively surface charged groups, which are most probably amine groups. As the pH decreases from this point, the base surface groups protonate, thus generating electropositive potential at the cell surface. It is interesting to note that at a pH of between 7 and 8, the surfaces of picocyanobacteria in natural water will carry a negative charge. Electrostatic interaction between cells and metal cations promotes adhesion to the bacteria surface. Further studies are necessary to quantify the adsorption of metals onto the cell surface.

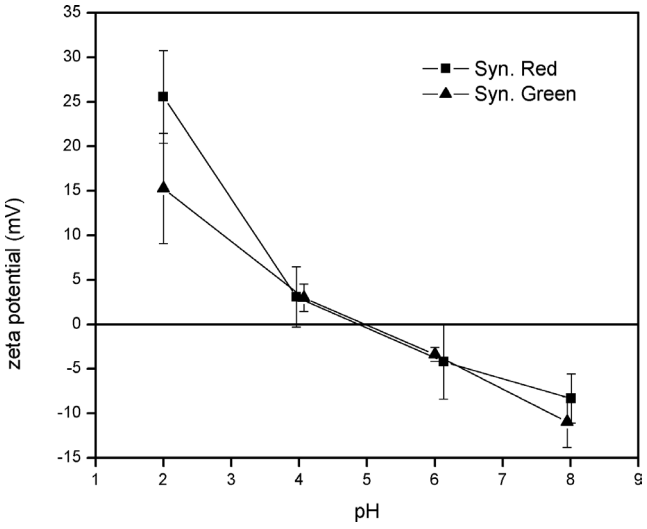

Fig. 1. Zeta potentials of two picocyanobacterial strains in 0.1 M $NaNO_3$ as a function of pH.

3.2. Potentiomentric titrations

Fig. 2 shows the titration curves for *Syn*. Green cells following the transformation to the charge balance expression of four replicate titrations. Consistent trends are observed for the titration curves in each set. These results demonstrate that while some surface variability can occur with the same bacterial strain (analogous to aging or subtle preparatory differences for mineral solids), reproducible quantitative titration curves for estimates of surface characteristics can be obtained.

The titration curves in Fig. 3 are displayed in comparison to the titration of the electrolyte. It is clear that the presence of bacteria influences the buffering capacity of the electrolyte. This buffering is due to the functional groups on the bacterial surface, which consume added base by losing their protons. However, the bacterial suspension displays relatively weak inflection points. This behavior has been attributed to the existence of several functional groups with an overlapping range of pH over which they deprotonate [32].

The results of the titration experiments were used to generate an optimal description of the numbers, concentra-

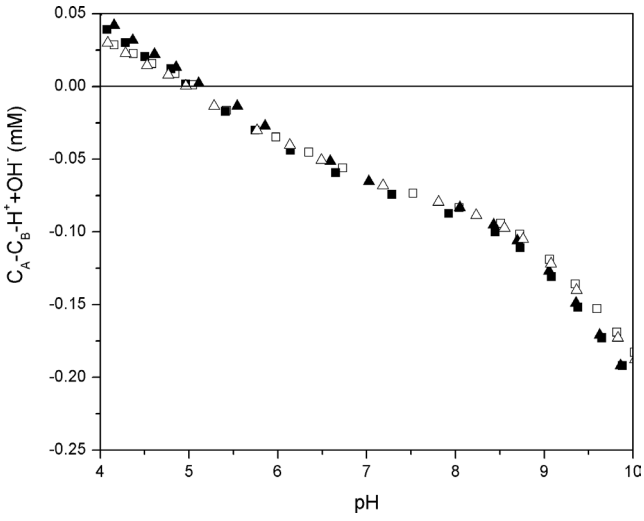

Fig. 2. H^+ exchanged for four replicate acid–base titrations of *Syn*. Green from the same population (0.26 g/l) in 0.1 M $NaNO_3$. Closed symbols correspond to the forward titration data and open symbols correspond to the back titration.

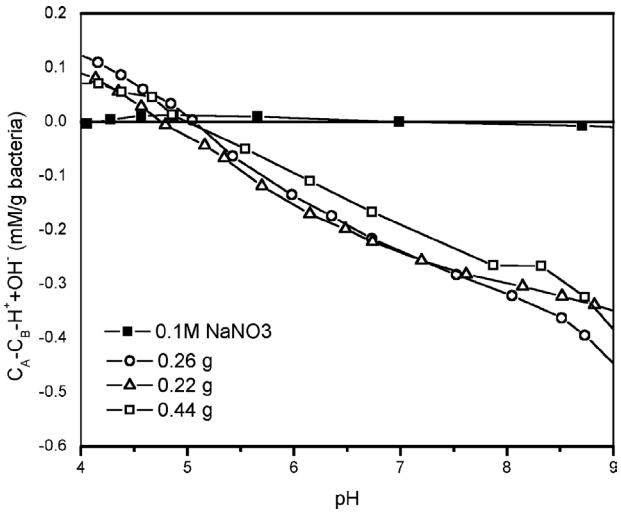

Fig. 3. Acid–base titration data from the titration performed using *Syn*. Green. Also shown is the titration curve for the electrolyte in the absence of bacteria.

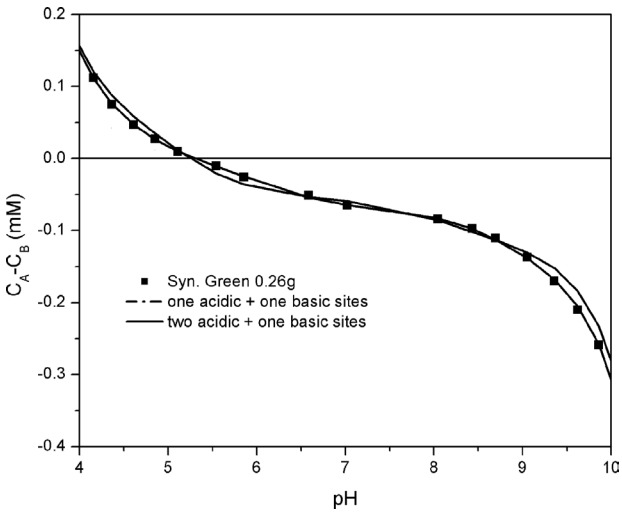

Fig. 4. Potentiometric titration curve for *Syn*. Green at 0.26 g/l. Also shown are FITEQL regressions (lines connecting data points) for different models of the cell surface. The dot–dash line corresponds to the model based on one acidic and one basic site. The solid line corresponds to the three sites model based on two acidic sites and one basic site.

tions, and thermodynamic properties of ionizable functional groups on the bacterial surface.

Specific adsorption of electrolyte ions onto the bacterial surface was not considered, as it would require titration experiments over a range of several orders of magnitude with respect to electrolyte concentration. The bacterial surface, however, reacts sensitively to extreme shifts of salinity: cells may undergo spontaneous lysis in solutions with low ionic strength, while the membrane-mounted proteins tend to solubilize at significantly higher ionic strengths [33,34].

3.3. Functional groups on the cell surface

Table 1 summarizes the results of FITEQL optimizations for the titrations of two picocyanobacterial strains based on two-site (acidic and basic site) and three-site models (two acidic sites and one basic site). Proton dissociation from the cell surface can be described by the reactions

$$S_1H \leftrightarrow >S_1^- + H^+ \text{ (acid reaction)}$$

and

$$S_2H^+ \leftrightarrow >S_2 + H^+ \text{ (base reaction)},$$

where $>S_1$ and $>S_2$ represent the acid- and base-type sites of bacteria, respectively.

The results obtained with this approach reflect the average properties of a heterogeneous population of functional units. The calculated parameters behave as if they were of a single functional type. This simple approach was successfully applied to titration studies on Gram-positive bacteria [12,13] and Gram-negative bacteria [18,23,25].

The models that considered the cell surface as a monoprotic acid or base failed to reproduce the titration data. A model separating two discrete sites with acidic and basic properties converges for the titration data. A three-site model (two acidic groups and one basic group) provided an improved fit to the titration data compared with the previous model (Fig. 4, Table 1). This observation is consistent with results from previous studies on Gram-positive and Gram-negative bacteria (see reviews in [20,23]). Cox et al. [35] and Sokolov et al. [24] proposed a five-site model based on discrete affinity spectra for Gram-positive *Bacillus* and Gram-negative *Shewanella putrefaciens*. However, Cox et al. [35] suggested that two of their distinct sites could be of the same functional group, which they assigned to carboxyl moieties. Sokolov et al. [24] proposed the presence of phosphodiester sites at low pH with separate pK_a values for amine and hydroxyl groups at higher pH. Conversely, Pagnanelli et al. [36] identified only two groups on the surface of *Arthrobacter* sp. ($pK_1 = 6.9$ and $pK_2 = 10.1$), which they assigned to phosphoryl and amine groups.

Results obtained for two bacterial strains are shown in Table 2, along with data from other studies. Through comparison of the mean pK_a values of three sites in the present strains of *Syn*. Green and Red with those from previous studies [20,35] and from known functional groups, sites with $pK_1 = 4.8$ and 5.0 can be assigned to carboxyl ($pK_a = 2$–6), while those with $pK_2 = 6.6$ and 6.7 are assigned to phos-

Table 1
Deprotonation constants as calculated by FITEQL 4 [28]

Model	pK_i of sites i							
	Syn. Green				*Syn*. Red			
	pK_1	pK_2	pK_3	$V(Y)$[a]	pK_1	pK_2	pK_3	$V(Y)$[a]
2 sites:								
1 acidic + 1 basic	5.05	6.66	–	11	5.11	7.56	–	13
3 sites:								
2 acidic + 1 basic	4.85	6.56	8.76	3	4.98	6.69	8.66	5

[a] Variance as calculated by FITEQL; see Eq. (1). A value range of $0.1 < V(Y) < 20$ represents a good fit.

Table 2
Comparison of deprotonation constants in 0.1 M $NaNO_3$ between the present strains and other strains of bacteria for which data is available

Reference	Species	n[a]	pK_1	pK_2	pK_3
This study	*Syn*. Green	4	4.85 ± 0.31	6.56 ± 0.2	8.76 ± 0.06
	Syn. Red	4	4.98 ± 0.16	6.69 ± 0.39	8.66 ± 0.21
[23]	Unknown Gram-negative	6	4.3 ± 0.2	6.9 ± 0.5	8.9 ± 0.5
[25]	*S. putrefaciens*, Gram-negative	3	5.16 ± 0.04	7.22 ± 0.15	10.04 ± 0.67
[20]	Calotrix cell		4.7 ± 0.4	6.6 ± 0.2	9.1 ± 0.3
	Calotrix sheath		4.8 ± 0.3	6.5 ± 0.1	8.7 ± 0.2
[12]	*B. subtilis*, Gram-positive	18	4.8 ± 0.14	6.9 ± 0.5	9.4 ± 0.6

[a] Number of titration experiments.

phoryl ($pK_a = 5.6$–7.2). The remaining values of $pK_3 = 8.8$ and 8.7 in the *Syn*. Green and Red strains, respectively, are within the ranges of phenolic (hydroxyl, $pK_a = 8$–12) and amine ($pK_a = 8.6$–9.0) groups.

3.4. Concentrations of surface sites

It has been shown that surface site densities can vary significantly depending on the growth phase of bacteria; i.e., the exponential phase yields higher site concentrations than either stationary or sporulated phases [37]. Haas et al. [25], however, recently demonstrated that the acid–base behavior of the Gram-negative *Shewanella putrefaciens* is largely insensitive to variations in culture age and media composition. The cells in our study were harvested following three days in the stationary phase, similarly to the growth phase of other studies in Table 3.

When compared with *Syn*. Green, *Syn*. Red has a higher total site concentration (16.6×10^{-4} mol/g), which is slightly higher than that of the Gram-negative strain *Calotrix* (14.6×10^{-4} mol/g) [38], as well as an unknown strain from the genus *Enterobacteriaceae* (12.7×10^{-4} mol/g) [23]. The overall pH-buffering capacity of other picocyanobacteria strains appears to be of the same order of magnitude as that of other Gram-negative bacteria (Table 3). The lowest values were those reported by Haas et al. [25] for *Shewanella putrefaciens*, although Sokolov et al. [24] reported a value of 17.7×10^{-4} mol/g for the same strain. Gram-positive cells have been expected to possess more buffering capacity than their Gram-negative counterparts because the Gram-positive cell envelope is surrounded by a thick external layer of peptidoglycan (PG). The PG layer in Gram-negative cells is much thinner than what is typical for Gram-positive bacteria. In Gram-negative cells, the PG is surrounded by an outer membrane, the outer aspect of which is composed largely of lipopolysaccharide (LPS). The latter is thought to play an important role in metal binding to the cell exterior [25,39]. It can be shown that the two Gram-positive bacteria, *Bacillus licheniformis* and *Bacillus subtilis*, have higher total site concentrations when compared with some Gram-negative strains.

Although the total site densities for all investigated strains are of the same order of magnitude (implying similarities in total surface site densities), the distribution between the functional groups appears to be individual for each strain. The estimated size concentrations obtained from the one base–two acid site (b–a–a) model were normalized with dry mass of bacteria in each titration to yield surface site densities, which were $2.6 \pm 0.4/7.4 \pm 1.6$ (carboxyl site), $1.9 \pm 0.5/4.4 \pm 0.8$ (phosphoryl site), and $2.5 \pm 0.4/4.8 \pm 0.7$ (amine/hydroxyl site) 10^{-4} mol/g, respectively. Table 3 displays a compilation of site densities determined for the present strain, along with data from the literature on other strains [23]. Site densities are provided in terms of moles of sites per gram of bacteria (Table 3).

Daughney and Fein [13] found that different strains of Gram-positive bacteria *Bacillus* possess carboxyl site densities in a range of 8.9–12.0×10^{-4} mol/g bacteria. Haas et al. [25] estimated a carboxyl density of 0.3×10^{-4} mol/g for *S. putrefaciens*, compared with our estimated range of 2.6–7.4×10^{-4} mol/g for the strains.

Our estimate of the concentration of phosphoryl groups on the picocyanobacteria surface (1.9–4.4×10^{-4} mol/g) is similar to that known from previous studies on Gram-negative bacteria (Table 3). According to Daughney and Fein [13] and Fein et al. [12], Gram-positive bacteria posses higher phosphoryl groups (4.4–8.3×10^{-4} mol/g). It is interesting to note that the pK_2 value is also similar in all studies [23].

Both amine and hydroxyl groups may be responsible for the estimated pK_3 values. The total surface charge estimated from the concentrations of surface groups is slightly negative with pH values between 4 and 5 in the presence of hydroxyl groups (Table 2). However, the zeta measurements showed that the cell surface is positively charged at $pH < 5$, leading to the conclusion that the third functional group should consist of an amine group.

Our investigation indicates an amine group component to pH buffering that has been previously unreported for Gram-positive *Bacillus* [12] and observed for Gram-negative *Shewanella* [25]. The amine site concentration density is higher (2.5–4.8×10^{-4} mol/g) than that of *Shewanella* [25] (Table 3). Borrok et al. [21] showed that acid washing similar to that in the experiments of Yee and Fein [18] irreversibly affects the cell wall. Consequently, the adsorbance capacity of Gram-negative bacteria may be overestimated.

Finally, the majority of previous studies have also used freeze-dried cells, with the exception of those from Fein et

Table 3
Comparison of surface site concentrations in 0.1 M $NaNO_3$ between the present strains and other strains of bacteria for which data are available

Reference	Species	C_{tot}	C_1	C_2	C_3
This study	*Syn.* Green, Gram-negative	6.9	2.6 ± 0.4	1.9 ± 0.5	2.5 ± 0.4
	Syn. Red, Gram-negative	16.6	7.4 ± 1.6	4.4 ± 0.8	4.8 ± 0.8
[23]	Enterobacteriaceae, Gram-negative	12.7	5.0 ± 0.7	2.2 ± 0.6	5.5 ± 2.2
[25]	*S. putrefaciens*, Gram-negative	0.78	0.32 ± 0.02	0.09 ± 0.01	0.38 ± 0.01
[20]	Calotrix cell, Gram-negative	14.6	3.28 ± 0.27	4.14 ± 0.31	7.16 ± 0.97
	Calotrix sheath	1.83	0.46 ± 0.17	0.45 ± 0.09	0.92 ± 0.22
[12][a]	*B. subtilis*, Gram-positive	22.6	12 ± 1	4.4 ± 0.2	6.2 ± 0.2
[13][a]	*B. licheniformis*, Gram-positive	29.9	8.9 ± 3.8	8.3 ± 4.6	12.7 ± 6.8

Note. Concentrations of the surface sites expressed as 10^{-4} mol/g of dry bacterial biomass.
[a] Reported in Ngwenya et al. [23], recalculated to g of dry weight of bacteria.

al. [12]. Daughney and Fein [13] and Ngwenya et al. [23] found that the use of wet or freeze-dried cells does not produce different results. Our results demonstrate that picocyanobacteria posses a significant number of functional groups on their cell surfaces. As picocyanobacteria can dominate phytoplankton communities in freshwater or marine systems, they may play an important role in adsorption of metals in those environments.

3.5. Infrared spectroscopy

The ATR-IR spectra contain information on the molecular level of functional groups present on cells. Despite the complexity of spectra, some characteristic peaks can be assigned. The infrared bands are composed of a combination of peaks from protein, lipid, and carbohydrate functional groups. The spectral features for bacterial cells are well established [40,41]. Recently, infrared bands of cyanobacteria have been investigated (e.g., *Synechococcus* PCC 7942 [42] and filamentous *Calothrix* sp. [20,43]).

The investigated strains in this study are *Synechococcus* types of picocyanobacteria. In order to compare the IR spectra of the investigated strains with the known data from literature, we measured the IR spectrum of *Synechococcus* PCC 7942. This spectrum is added to Fig. 5, which shows the IR spectra of *Syn.* Green and Red.

The functional groups of cyanobacteria and corresponding infrared frequencies are summarized in Table 4. It must be taken into account that a clear distinction between cell surfaces and the inner cell is not possible. The ATR-IR beam penetrates approximately 5 μm into the material, which is similar to the diameter of cyanobacteria.

Examination of spectra reveals both the similarities of spectra and a number of spectral regions, which can account for the chemical differences between the strains. In the region 2000–1500 cm^{-1} the spectra are dominated by absorbance from the peptide backbone [43]. The amide I group presents characteristic absorption at approximately 1650 cm^{-1} (C=O stretching), while the amide II group was observed at approximately 1540 cm^{-1}. These two features are very characteristic for cyanobacterial cells [42,43] and were also found in this study. Also interesting to note, that

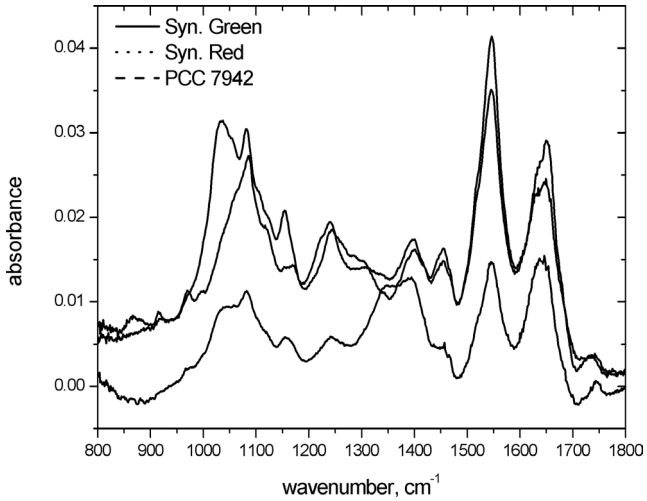

Fig. 5. Infrared spectra of PCC 7942, *Syn.* Green and *Syn.* Red collected in 0.1 M $NaNO_3$ electrolyte solution. See Table 4 for specific band assignments.

the two amide bands were observed in spectra of the freeze-dried oral streptococcal strains cells [17].

The peaks near 1400 cm^{-1} are characteristic of symmetric vibration versus COO-frequencies of amino acid side chains and free fatty acids. The amide III group was found in PCC 7942 and *Syn.* Green at approximately 1455 cm^{-1} but seems to be concealed by strong polysaccharide vibrations in *Syn.* Red. The most significant differences occur within the range 1200–1500 cm^{-1}. Absorption at approximately 1242 cm^{-1} corresponds to the asymmetric phosphodiester stretching (P=O) of the nucleic acids [40]. This feature is very pronounced in spectra of PCC 7942 and *Syn.* Green, but overlapped in the *Syn.* Red spectrum. Another nucleic acid phosphodiester peak at 1080 cm^{-1} (symmetric stretch P=O) is represented in all spectra, although at this region (1200–900 cm^{-1}) the stretching (C–O–C) vibrations of polysaccharides (glycogen) dominate the absorbance.

Below 2000 cm^{-1} the main lipid band can be found at approximately 1740 cm^{-1} (C=O ester stretching vibrations) and is derived primarily from the ester linkage of the fatty acids (aliphatic monocarboxylic acids). FTIR spectra contain prominent features derived from carbohy-

Table 4
List of band assignments

Wavenumber (cm^{-1})	Assignment	Comments
~ 1740	ν>C=O of ester functional groups primarily from membrane lipids and fatty acids [46]	
~ 1650	νC=O of amides associated with proteins [47,48]	Usually called the amide I band
~ 1540	δN–H of amides associated with proteins [47,48]	Usually called the amide II band, may also contain contributions from C=N stretches
~ 1455	$\delta_{ac}CH_2/\delta_{ac}CH_3$ of proteins [49]	The positions of these broad peaks vary in the literature, called the amine III band
~ 1398	$\delta_{ac}CH_2/\delta_{ac}CH_3$ and ν_sC–O of carboxylic groups [47,49]	The positions of these assignments vary in the literature
~ 1240	ν_{as}P=O of the phosphodiester backbone of nucleic acid (DNA and RNA)	General phosphoryl groups
~ 1200–900	νC–O–C of polysaccharides [49,50], ~ 1165, ~ 1110, 1050, 1030 for C–O	The predominant polysaccharide in cyanobacteria is glycogen
~ 1080	ν_sP=O of the phosphodiester backbone of nucleic acid (DNA and RNA) [47,50]	May also be due to the presence of phosphorylated proteins and polyphosphate storage products

drate adsorption bands that spread over approximately 300 wave numbers from 1200 to 900 cm^{-1} (at approximately 1165 and 1030 cm^{-1}). Although the spectra of *Syn*. Green and *Syn*. Red are similar to those obtained with filaments from the cyanobacteria *Calothrix* sp. (size of 1 mm × 5 µm thick) [20], specific features occur between 1500 and 1200 cm^{-1}.

FTIR spectroscopy of freeze-dried cells was found to be a sensitive tool for the study of microbial cell surfaces [44]. Recently, FTIR spectroscopy was applied for the identification and characterization of bacteria suspension (see [42] and references therein). It was shown that the IR spectrum is unique to certain strains. However, it is still unclear whether biochemical changes in the growth stage cause different IR spectra and how sensitive IR spectra reflect the protonation or deprotonation process.

Haas [45] revealed that media composition and culture age do not influence the acid–base behavior of Gram-negative bacteria *Shewanella*. However, differences in deprotonation constants and the concentrations of functional groups arise when culture conditions were changed from aerobic to anaerobic.

By combining the IR data with comparisons of pK_a values of functional groups, tentative assignments of functional group identity can be made. On the cell surface of both picocyanobacteria strains we hypothesize the presence of carboxyl groups ($pK = 4.85$, 4.98), phosphoryl groups ($pK = 6.56$, 6.69), and amine groups ($pK = 8.76$, 8.66).

The overlap in deprotonation constants across the two strains, coupled with similarities in the magnitude of total surface densities, suggest that a common surface chemistry may be used in biogeochemical models involving cyanobacteria, thereby simplifying the modeling tasks.

4. Summary

In this study, the surface properties of two picocyanobacteria strains from two lakes were experimentally examined by measurements of zeta potential, potentiometric titration, and infrared spectroscopy. The results demonstrated that the deprotonation of picocyanobacterial cells surface is a reversible process. Modeling results, data on zeta potential and IR spectra are consistent with the presence of three distinct surface sites on the bacterial surface, corresponding to carboxyl, phosphate, and amine groups with a total concentration of 7–17 × 10^{-4} mol/g. The carboxyl group dominates the surface sites in both *Syn*. Green and *Syn*. Red strains with 37 and 44%, respectively, although the amine groups represent 36 and 29% as well. The smaller fraction of phosphate was similar in both strains with 27 and 26%. Our results on the deprotonation constants for the different sites are consistent with the findings of other studies.

During the picocyanobacterial bloom (cell numbers about 3.4 × 10^5 cells/ml) in oligotrophic lakes, the total concentration of functional groups amounts to 3.5 × 10^{-4} mmol/l. The zeta potential measurements have shown that picocyanobacteria are negatively charged at a pH range between 6 and 7, which is typical for natural surface water. Calcium cations can therefore be easily attracted. On the other hand, the presence of amine groups on the cell surface influences the carbonate anions. Both reactions are important in the nucleation of calcite on the cell and may be key processes for the calcite precipitation in lakes.

Due to the dominance of carboxyl groups on the cell surface, picocyanobacteria can play an important role in metal cycling in aquatic systems. For that reason, picocyanobacteria have a general potential for applications such as reducing metal concentrations at polluted sites. However, reaping this

potential requires further investigation of the cell surface characteristics and the development of techniques to effectively cultivate picocyanobacteria.

Acknowledgments

This research has been partially supported with funding from Swiss Federal Institute of Technology, ETH. We thank S. Peiffer for making it possible to carry out the zeta measurements in his department. We acknowledge Stephan Hug for introducing us to ATR-IR spectroscopy and helping with measurements. We also thank B. Wehrli and two anonymous reviewers for their constructive comments, which helped us to clarify our arguments.

References

[1] J.G. Stockner, Limnol. Oceanogr. 4 (Part 2) (1988) 765.
[2] F. Partensky, W.R. Hess, D. Vaulot, Microbiol. Mol. Biol. Rev. 63 (1999) 106.
[3] T. Weisse, in: J.G. Jones (Ed.), in: Advances in Microbial Ecology, vol. 13, Plenum, New York, 1993, p. 327.
[4] J. Stockner, C. Callieri, G. Cronberg, in: B.A. Whitton, M. Potts (Eds.), The Ecology of Cyanobakteria, Kluwer Academic, Dordrecht, 2000, p. 195.
[5] N.S.R. Agawin, C.M. Duarte, S. Agusti, Limnol. Oceanogr. 3 (2000) 591.
[6] T. Bell, J. Kalff, Limnol. Oceanogr. 46 (2001) 1243.
[7] J.A. Raven, Funct. Ecol. 12 (1998) 503.
[8] M. Dittrich, P. Kurz, B. Wehrli, Geomicrobiology 21 (2004) 45.
[9] J.B. Thompson, F.G. Ferris, Geology 18 (1990) 995.
[10] M. Obst, M. Dittrich, H. Kuehn, Presented at the AGU Fall Meeting 2004, December 13–17, San Francisco, 2004.
[11] W. Hodgkiss, J.M. Shewan, in: M.R. Drop, E.J.F. Wood (Eds.), Advances in Microbiology of Sea, Academic Press, San Diego, 1968, p. 127.
[12] J.B. Fein, C.J. Daughney, N. Yee, T.A. Davis, Geochim. Cosmochim. Acta 61 (1997) 3319.
[13] C.J. Daughney, J.B. Fein, J. Colloid Interface Sci. 198 (1998) 53.
[14] D.A. Fowle, J.B. Fein, Geochim. Cosmochim. Acta 63 (1999) 3059.
[15] A.C.C. Plette, M.F. Benedetti, W.H. van Riemsdik, Environ. Sci. Technol. 30 (1996) 1902.
[16] R.E. Martinez, F.G. Ferris, J. Colloid Interface Sci. 243 (2001) 73.
[17] H.C. van der Mei, R. Bos, H.J. Busscher, Colloid Surf. B Biointerfaces 11 (1998) 213.
[18] N. Yee, J. Fein, Geochim. Cosmochim. Acta 65 (2001) 2037.
[19] T.J. Beveridge, R.J. Doyle, Metal Ions and Bacteria, Wiley, New York, 1989.
[20] N. Yee, L.G. Benning, V.R. Phoenix, F.G. Ferris, Environ. Sci. Technol. 38 (2004) 775.
[21] D. Borrok, J.B. Fein, M. Tischler, E. O'Loughlin, H. Meyer, M. Liss, K.M. Kemner, Chem. Geol. 209 (2004) 107.
[22] R.E. Martinez, K. Pedersen, F.G. Ferris, J. Colloid Interface Sci. 275 (2004) 82.
[23] B.T. Ngwenya, I.W. Sutherland, L. Kennedy, Appl. Geochem. 18 (2003) 527.
[24] I. Sokolov, D.S. Smith, G.S. Henderson, Y.A. Gorby, F.G. Ferris, Environ. Sci. Technol. 35 (2001) 341.
[25] J.R. Haas, T.J. Dichristina, R. Wade, Chem. Geol. 180 (2001) 33.
[26] H.C. van der Mei, J. de Vries, H.J. Busscher, Surf. Sci. Rep. 39 (2000) 3.
[27] K.C. Marshall, R.S. Pembrey, R.P. Schneider, Colloids Surf. B Biointerfaces 2 (1994) 371.
[28] A.L. Herbelin, J.C. Westall, FITEQL 4.0—A Computer Program for Determination of Chemical Equilibrium Constants from Experimental Data, Report 99-01. Department of Chemistry, Oregon State University, Corvallis, OR, 1999.
[29] E.M. Sonnenfeld, T.J. Beveridge, A.L. Koch, R.J. Doyle, J. Bacteriol. 163 (1985) 1167.
[30] A.R. Shashikala, A.M. Raichur, Colloids Surf. B Biointerfaces 24 (2002) 11.
[31] N. Yee, D.A. Fowle, F.G. Ferris, Geochim. Cosmochim. Acta 68 (2004) 3657.
[32] H. Seki, A. Suzuki, S. Mitsueda, J. Colloid Interface Sci. 197 (1998) 185.
[33] M.T. Madigan, J.M. Martinko, J. Parker, Biology of Microorganisms, Prentice Hall, New York, 2000.
[34] D. Voet, J.G. Voet, Biochemistry, Wiley, New York, 1995.
[35] J.S. Cox, D.S. Smith, L.A. Warren, F.G. Ferris, Environ. Sci. Technol. 33 (1999) 4514.
[36] F. Pagnanelli, M.P. Papini, L. Toro, M. Trifoni, F. Veglio, Environ. Sci. Technol. 34 (2000) 2773.
[37] C.J. Daughney, D.A. Fowley, D. Fortin, Geochim. Cosmochim. Acta 65 (2001) 1025.
[38] N. Yee, J.B. Fein, Geomicrobiology 20 (2003) 43.
[39] S. Langley, T.J. Beveridge, Can. J. Microbiol. 45 (1999) 616.
[40] D. Naumann, C. Schultz, D. Helm, in: H.H. Mantsch, D. Chapman (Eds.), Infrared Spectroscopy of Biomolecules, Wiley–Liss, New York, 1996, p. 279.
[41] H. Gremlich, B. Van, Infrared and Raman Spectroscopy of Biological Materials, Dekker, New York, 2000.
[42] M. Kansiz, P. Heraud, B. Wood, F. Burden, J. Beardall, D. McNaughton, Phytochemistry 52 (1999) 407.
[43] L.G. Benning, V.R. Phoenix, N. Yee, M.J. Tobin, Geochim. Cosmochim. Acta 68 (2004) 729.
[44] H.C. van der Mei, J. Noordmans, H.J. Busscher, Biochim. Biophys. Acta 991 (1989) 395.
[45] J.R. Haas, Chem. Geol. 209 (2004) 67.
[46] D.B. Hedrick, D.E. Nivens, C. Stafford, D.C. White, J. Microbiol. Methods 13 (1991) 67.
[47] W.H. Nelson, Modern Techniques for Rapid Microbiological Analysis, VCH, New York, 1991.
[48] D.H. Williams, I. Fleming, Spectroscopic Methods in Organic Chemistry, McGraw–Hill, London, 1995.
[49] W. Zeroual, M. Manfait, C. Choisy, Pathol. Biol. 43 (1995) 300.
[50] P.T.T. Wong, R.K. Wong, T.A. Caputo, T.A. Godwin, B. Rigas, Proc. Natl. Acad. Sci. USA 88 (1991) 10,988.